Mechanical ventilation triggers abnormal mitochondrial dynamics and morphology in the diaphragm

Martin Picard, Ilan Azuelos, Boris Jung, Christian Giordano, Stefan Matecki, Sabah Hussain, Kathryn White, Tong Li, Feng Liang, Andrea Benedetti, et al.

Mechanical ventilation triggers abnormal mitochondrial dynamics and morphology in the diaphragm

Martin Picard,[1] Ilan Azuelos,[2,4] Boris Jung,[2,3] Christian Giordano,[2] Stefan Matecki,[3] Sabah Hussain,[2,4] Kathryn White,[5] Tong Li,[2] Feng Liang,[2] Andrea Benedetti,[6] Benoit J. Gentil,[7] Yan Burelle,[8] and Basil J. Petrof[2,4]

[1]*Center for Mitochondrial and Epigenomic Medicine, The Children's Hospital of Philadelphia and University of Pennsylvania, Philadelphia, Pennsylvania;* [2]*Meakins-Christie Laboratories, McGill University Health Centre Research Institute, Montreal, Quebec, Canada;* [3]*Department of Critical Care Medicine and Anesthesiology, Saint Eloi Teaching Hospital, and Centre National de la Recherche Scientifique, Institut National de la Santé et de la Recherche Médicale (INSERM U-1046), Montpellier University, Montpellier, France;* [4]*Critical Care and Respiratory Divisions, McGill University Health Centre, Montreal, Quebec, Canada;* [5]*EM Research Services, Newcastle University, Newcastle upon Tyne, United Kingdom;* [6]*Department of Medicine and Department of Epidemiology, Biostatistics & Occupational Health, McGill University, Montreal, Quebec, Canada;* [7]*Department of Neurology/Neurosurgery and Montreal Neurological Institute, McGill University, Montreal, Quebec, Canada; and* [8]*Faculty of Pharmacy, Université de Montréal, Montreal, Quebec, Canada*

Picard M, Azuelos I, Jung B, Giordano C, Matecki S, Hussain S, White K, Li T, Liang F, Benedetti A, Gentil BJ, Burelle Y, Petrof BJ. Mechanical ventilation triggers abnormal mitochondrial dynamics and morphology in the diaphragm. *J Appl Physiol* 118: 1161–1171, 2015. First published March 12, 2015; doi:10.1152/japplphysiol.00873.2014.—The diaphragm is a unique skeletal muscle designed to be rhythmically active throughout life, such that its sustained inactivation by the medical intervention of mechanical ventilation (MV) represents an unanticipated physiological state in evolutionary terms. Within a short period after initiating MV, the diaphragm develops muscle atrophy, damage, and diminished strength, and many of these features appear to arise from mitochondrial dysfunction. Notably, in response to metabolic perturbations, mitochondria fuse, divide, and interact with neighboring organelles to remodel their shape and functional properties—a process collectively known as mitochondrial dynamics. Using a quantitative electron microscopy approach, here we show that diaphragm contractile inactivity induced by 6 h of MV in mice leads to fragmentation of intermyofibrillar (IMF) but not subsarcolemmal (SS) mitochondria. Furthermore, physical interactions between adjacent organellar membranes were less abundant in IMF mitochondria during MV. The profusion proteins Mfn2 and OPA1 were unchanged, whereas abundance and activation status of the profission protein Drp1 were increased in the diaphragm following MV. Overall, our results suggest that mitochondrial morphological abnormalities characterized by excessive fission-fragmentation represent early events during MV, which could potentially contribute to the rapid onset of mitochondrial dysfunction, maladaptive signaling, and associated contractile dysfunction of the diaphragm.

mitochondrial dynamics; mitochondrial fragmentation; intermyofibrillar mitochondria; subsarcolemmal mitochondria; electron microscopy; ventilator-induced diaphragmatic dysfunction

MECHANICAL VENTILATION (MV) suppresses diaphragm contractile activity, leading to maladaptive changes in diaphragm structure and function (22, 25, 33, 43). This phenomenon is termed ventilator-induced diaphragmatic dysfunction (VIDD) (52) and has the potential to impede the ability to remove a patient from a ventilator, thereby contributing to greater medical complications and higher health care costs. The molecular events characterizing VIDD include oxidative stress (27, 36, 43, 47), mitochondrial energy deficiency (27, 43), activation of autophagy (23), apoptosis (35, 49), and increased activation of proatrophy signaling pathways (32, 33). Importantly, all of these cellular processes can be either directly or indirectly induced by mitochondrial dysfunction, which occurs in the inactive diaphragm within a short period of time (a few hours in animal models, a few days in humans) after the initiation of MV (27, 43). Therefore, rapidly acquired mitochondrial dysfunction during MV may represent a key early cellular trigger for the development of VIDD.

Skeletal muscle fibers contain two pools of mitochondria: intermyofibrillar (IMF) and subsarcolemmal (SS) mitochondria. IMF mitochondria normally exist as tubular and branched organelles (i.e., mitochondrial reticulum) surrounding myofibrils in tridimensional space, whereas SS mitochondria are more spheroid-shaped and are located between the plasma membrane and myofibrils (4, 46). Importantly, IMF and SS mitochondria exhibit different functional characteristics with respect to oxidative capacity, reactive oxygen species (ROS) generation, and sensitivity to the proapoptotic event of mitochondrial permeability transition pore opening (11, 41), which could have implications in disuse-associated diaphragmatic dysfunction.

Mitochondria have the ability to undergo remodeling through fusion, fission, and interactions with neighboring mitochondria as well as with other organelles, a process collectively referred to as mitochondrial dynamics (8, 51). In cultured cells, effector proteins of mitochondrial dynamics induce changes in mitochondrial shape within seconds to minutes, which has consequences for mitochondrial function [reviewed in (45)]. For example, loss of function of the mitochondrial profusion proteins mitofusin 2 (Mfn2) and optic atrophy 1 (OPA1) favors the accumulation of mitochondrial DNA damage (10, 40) and decreased mitochondrial bioenergetic efficiency with impaired energy production capacity (5, 9). These effects appear to be at least partly related to the fact

Address for reprint requests and other correspondence: B. J. Petrof, Meakins-Christie Laboratories, McGill University Health Centre Research Institute (Block E), 1001 Decarie Boulevard, Montreal, Quebec, Canada H4A 3J1 (e-mail: basil.petrof@mcgill.ca).

that mitochondrial fusion enables functional complementation via sharing of proteins, RNA, and DNA (10, 40). On the other hand, mitochondrial fragmentation triggered by excessive activation of the profission protein dynamin-related protein 1 (Drp1) can lead to greater ROS production, loss of ATP production, and greater mitochondrial membrane depolarization (26, 31, 39, 56). Furthermore, dysregulation of mitochondrial dynamics and the resulting mitochondrial dysfunction can promote exaggerated apoptotic signaling (31, 39, 55) and activation of the muscle atrophy program (48).

Given that the functional consequences of exaggerated mitochondrial fission-fragmentation overlap closely with the main cellular mechanisms implicated in the development of VIDD, we hypothesized that mitochondria could undergo adverse morphological remodeling in the diaphragm during MV. In the present study, we employed a quantitative transmission electron microscopy (TEM) approach to determine the effects of MV on mitochondrial shape and membrane interactions (46) in the IMF and SS mitochondrial populations of the diaphragm. We also evaluated the effect of MV on canonical profusion (Mfn2, OPA1) and profission (Drp1) mitochondrial proteins known to mediate mitochondrial remodeling and interorganelle interactions. Our findings suggest that MV rapidly leads to an excess of fission-fragmentation events in IMF (but not SS) mitochondria resulting in a loss of their characteristic morphological specialization features, which could potentially contribute to the pathogenesis of VIDD.

METHODS

Animals. Male C57BL/6N mice 8–10 wk of age (Charles River Laboratories, Saint-Constant, QC) were used for our experiments. All mice were housed under a standard 12:12-h light-dark cycle with food and water available ad libitum for 72 h before the experiments. The study was approved by the McGill University Health Centre institutional ethics board in accordance with guidelines of the Canadian Council on Animal Care.

Mechanical ventilation protocol. Mice were subjected to 6 h of MV using the same protocol that had been shown to induce impaired diaphragmatic function, as previously described in detail (37). Briefly, mice were anesthetized by intraperitoneal (i.p.) injection of xylazine and pentobarbital sodium (50 mg/kg body wt) and then orotracheally intubated with a 22-gauge angiocatheter. No neuromuscular blocking agents were used. General care included continuous maintenance of body temperature using a homeothermic blanket control unit (Harvard Apparatus, Saint-Laurent, QC, Canada), and hourly i.p. injections of 0.05 to 0.10 ml of Ringer lactate solution to maintain hemodynamic stability and compensate for insensible losses. MV was performed with a small-animal ventilator (Minivent; Harvard Apparatus) using the following ventilator settings: fraction of inspired oxygen of 0.21 (room air), controlled volume mode with tidal volume of 10 μl/mg body wt, respiratory rate of 150–170 breaths/min, and positive end-expiratory pressure level of 3–4 cmH_2O achieved by placing the expiratory port under a water seal. MV parameters and anesthesia were adjusted to prevent spontaneous breathing efforts, which were assessed by regular observations of thoracoabdominal motion and the bubbling pattern of the underwater seal. Control mice did not undergo mechanical ventilation. To replicate the fact that mice undergoing MV for 6 h were not fed during this period, control mice were fasted for the equivalent time with access to water. All mice were euthanized by i.p. injection of pentobarbital sodium (50 mg/kg body wt) and cervical dislocation at the same time of day (between 2:00 and 4:00 P.M.).

Transmission electron microscopy. For TEM analysis, diaphragm muscle strips (~5 mm wide, ~15 mm long) were fixed in a 2% glutaraldehyde solution in 0.1 M cacodylate buffer (pH 7.4) and processed exactly as described in (46). Samples were postfixed in 1% osmium tetroxide and dehydrated with acetone before impregnation in resin. Smaller segments of diaphragms were then embedded either in cross-section (i.e., transverse) or longitudinal orientation in 100% resin. To verify orientation and section quality, 1-μm-thick sections were cut and stained with 1% toluidine blue in 1% borax. Ultrathin sections of 70 nm were subsequently cut using a diamond knife on a Leica EM UC7 ultramicrotome, stretched with chroloform, and mounted on Pioloform-filmed copper grids prior to staining with 2% aqueous uranyl acetate and lead citrate. Ultrathin sections were examined on a Phillips CM 100 Compustage (FEI) transmission electron microscope and digital micrographs were captured with a charge-coupled device camera (Advanced Microscopy Techniques, Woburn, MA). Tissues from four to five mice per group were analyzed in two separate batches.

Morphological analysis. For each animal, randomly selected mitochondria-rich oxidative muscle fibers were analyzed in both transverse and longitudinal sections as previously described in detail (46). Briefly, to analyze IMF mitochondrial morphology, muscles were sectioned in transverse (cross-section) orientation. To ensure optimal transverse orientation at the subcellular level, muscle fibers must be sectioned in a near-parallel orientation to the Z-line. This was consistently achieved by selecting for analysis myofibers presenting at least one but no more than two Z-lines separated by at least 10–15 μm. Obliquely sectioned myofibers with Z-lines appearing closer than 10 μm were not selected for analysis. A total of 1,011 (control) and 1,011 (MV) IMF mitochondria from 22–23 myofibers were thus analyzed by an observer who was blind to group identity. SS mitochondrial morphology was determined at ×19,000 magnification in the longitudinal orientation ($n = 3$ mice per group), for which 708 (control) and 537 (MV) SS mitochondria were similarly analyzed.

Mitochondrial shape descriptors and size measurements were determined using ImageJ software (version 1.42q; National Institutes of Health, Bethesda, MD) as previously described (46) by manually tracing the perimeter of IMF and SS mitochondria with clearly discernible outlines on TEM micrographs, as shown in Fig. 1*E*. Aspect ratio was computed as [(major axis)/(minor axis)] and reflects the length-to-width ratio; form factor [$(\text{perimeter}^2)/(4\pi \text{ surface area})$] reflects morphological complexity in terms of waviness and branching; roundness [$4(\text{surface area})/(\pi \text{ major axis}^2)$] is a two-dimensional index of sphericity; Feret's maximum and minimum diameters reflect the longest and shortest distances between outer boundaries of a mitochondrion (28). To produce frequency distributions of these morphological parameters, each mitochondrion was assigned to one of 20 bins.

To quantify interactions among IMF and SS mitochondria, micrographs of muscle from five mice per group photographed in longitudinal orientation were used at magnifications of ×13,500 for IMF and ×19,000 for SS. In the IMF compartment, a total of 689 (control) and 648 (MV) Z-lines possessing mitochondria on both sides, either as pairs of discrete organelles, as a continuous mitochondrion, or as interacting organelles joined by an electron-dense intermitochondrial junction (IMJ) (2, 44) were evaluated. The proportion of Z-lines spanned by continuous or interacting mitochondria is reported as a percentage of the total number of Z-lines analyzed. In addition, the proportion of electron-dense physical contact sites between adjacent mitochondria was determined as described previously (46) in 543 (control) and 726 (MV) pairs of IMF mitochondria, and 1,206 (control) and 921 (MV) pairs of SS mitochondria.

Western blot analysis. For protein analyses, the diaphragm muscle was harvested and snap-frozen in liquid nitrogen. Muscle lysates were mixed with sample buffer and boiled for 5 min before gel loading. The dilutions of primary and secondary antibodies were made according to the manufacturers' instructions. Quantification of specific protein bands was performed using the Odyssey Infrared Imaging System (LI-COR Biosciences, Lincoln, NE) using Ponceau red staining to

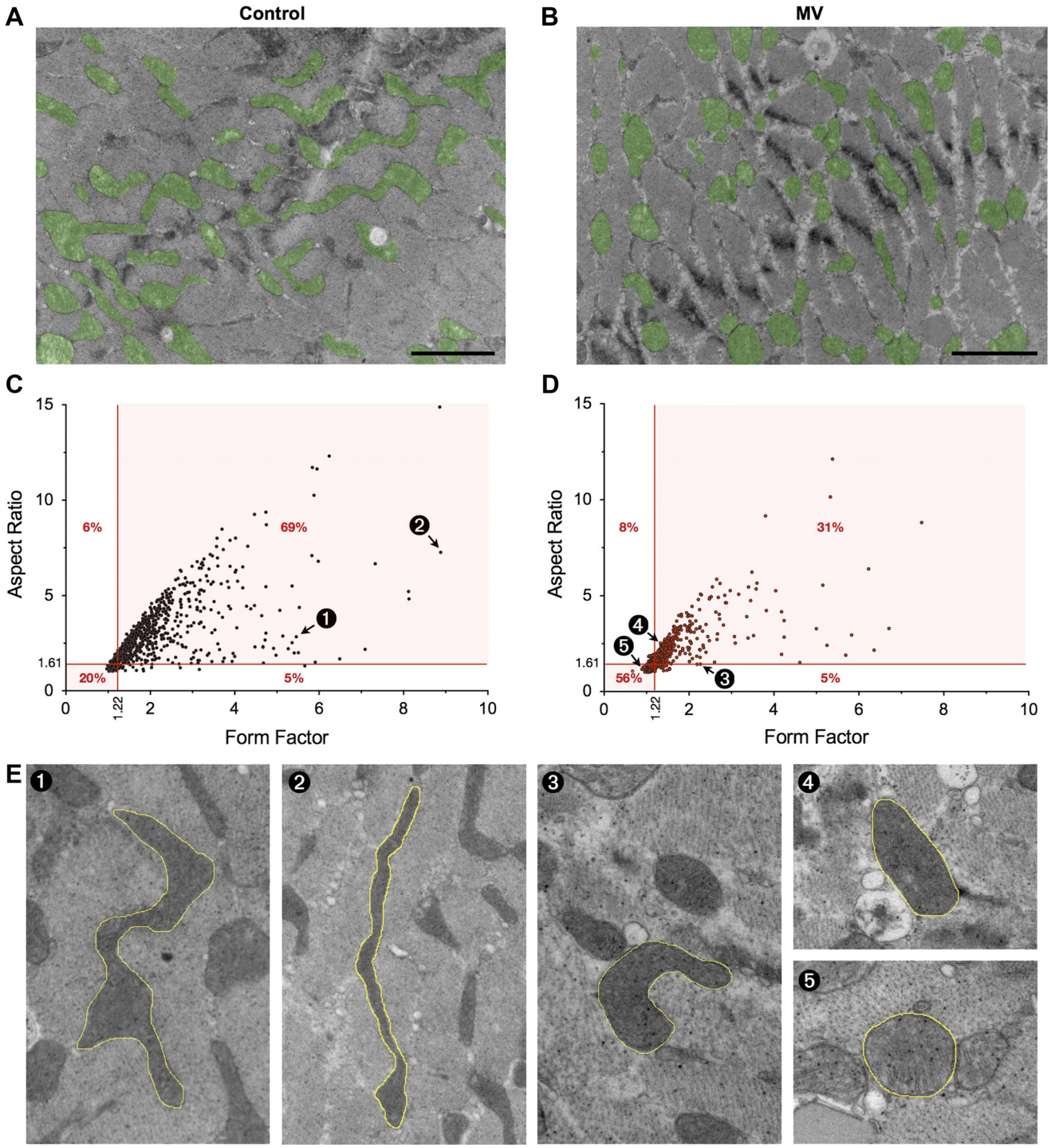

Fig. 1. Mechanical ventilation alters intermyofibrillar (IMF) mitochondrial morphology. Representative electron micrographs from control (*A*) and samples that underwent mechanical ventilation (MV) (*B*) with mitochondria pseudocolored in green (scale bars = 2 μm). Graphical representation of mitochondrial form factor (shape complexity) and aspect ratio (length to width ratio) from control (*C*) and MV (*D*) groups indicates less morphological complexity of MV mitochondria (n = 1,011 traced mitochondria for both groups). Percentages indicate proportions of mitochondria within each quadrant, defined by the 25th percentile of control mitochondria; the shaded quadrants contain mitochondria for which both parameters fall either below (left lower quadrant) or above (right upper quadrant) this threshold. *E*: representative morphology of mitochondrial subpopulations corresponding to the numbered data points in *C* and *D*.

adjust for any differences in total protein loading. The following proteins were detected: total Drp1 (611112, BD Biosciences), phosphorylated forms of Drp1 at serine 616 (pDrp1-616; 3455, Cell Signaling) and serine 637 (pDrp1-637; 6319, Cell Signaling), Mfn2 (M6319, Sigma), and OPA1 (MA5-16149, Thermo-Scientific).

Statistical analyses. Comparisons of morphological shape and size parameters between control and MV mitochondrial populations were made using a repeated-measures ANOVA. Distributions of these parameters were nonnormal, and hence, normalizing transformations were performed using either Johnson or Box-Cox methods, selected

on the basis of which method yielded the best residual plot distribution for the data. The significance of differences in mitochondrial population proportions falling above or below a predefined level was assessed using the z-test for proportions. Differences in mitochondrial interaction parameters and Western blot analysis quantifications between control and MV groups were evaluated by an unpaired, two-tailed Student's t-test assuming unequal variances, or the Mann-Whitney test in the case of nonparametric data (evaluated by the Anderson-Darling normality test). All statistical analyses were performed using Minitab 17 (Minitab) or Prism 6 (Graphpad) software with the alpha level set at 0.05.

RESULTS

IMF mitochondrial morphology. A representative example of IMF mitochondria in transverse section from a control diaphragm is shown in Fig. 1*A*. As can be seen, normal IMF mitochondria in the diaphragm are for the most part relatively elongated and wavy serpentine structures. In contrast, IMF mitochondria in the MV group diaphragm appear to be shorter with less branching and hence a less morphologically complex structure (Fig. 1*B*). Using the combined total IMF mitochondria from control (Fig. 1*C*) and MV (Fig. 1*D*) groups, dot plots of aspect ratio vs. form factor were generated and subdivided into four quadrants on the basis of 25th percentile values obtained for these two parameters in the control group. The IMF mitochondria falling in the lower left-hand quadrant of the dot plots (i.e., with <25th percentile values for both aspect ratio and form factor) were observed with greater frequency in the MV group (56%) compared with the control group (20%). Illustrative images of the individual marked mitochondria indicated by arrows in Fig. 1, *C* and *D* are shown in Fig. 1*E*.

To quantify these observations in greater detail, frequency distribution analyses of the total IMF mitochondrial populations in control and MV groups were individually determined for each of the following morphological parameters: aspect ratio (Fig. 2*A*), form factor (Fig. 2*B*), roundness (Fig. 2*C*), Feret's maximal (Fig. 2*D*) and minimal (Fig. 2*E*) diameters, and total perimeter (Fig. 2F). Using the median value obtained in the control group as a reference threshold for each parameter (hence by design 50% of the control population), greater percentages of IMF mitochondria in the MV group were observed with low values for aspect ratio, form factor, Feret's maximum diameter, and total perimeter. In addition, a slightly greater percentage of IMF mitochondria in the MV group demonstrated higher values for Feret's minimum diameter, which is in keeping with the elevated roundness values in this group. Table 1 shows mean and median values for these measurements in the control and MV groups. As indicated in Table 1, differences in IMF mitochondrial morphology between the control and MV groups were highly statistically significant as determined by repeated-measures ANOVA. Therefore, these data indicate that MV was associated with rapid remodeling of IMF mitochondria in the diaphragm, leading to a shift toward shorter, rounder, and less morphologically complex organelles within 6 h of initiating MV.

SS mitochondrial morphology. The same analyses were applied to SS mitochondria. Under baseline control conditions, SS mitochondria in the diaphragm are more spheroid and less morphologically complex than IMF mitochondria (Fig. 3*A*), which is also reflected by their smaller 25th percentile values for aspect ratio and form factor (Fig. 3*C*). The 25th percentile

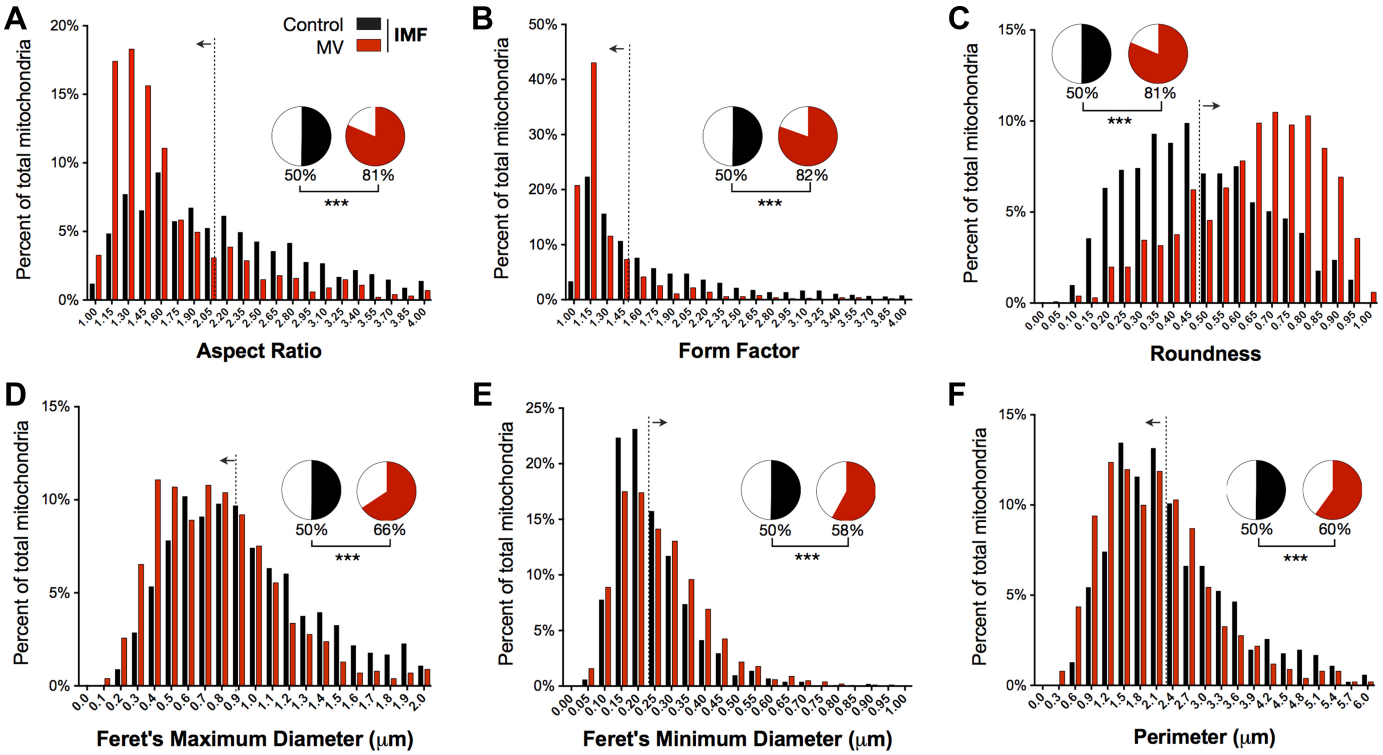

Fig. 2. MV fragments in IMF mitochondria. *A–F*: frequency distributions of the major IMF mitochondrial shape and size descriptors in diaphragms of control mice and those that underwent MV. Vertical dashed lines indicate the median value for each descriptor in the control group. Arrows adjacent to vertical dashed lines indicate the direction of change in each descriptor following MV, and pie charts show proportions of mitochondria falling to the arrow side of the dashed line in each experimental group. ***$P < 0.001$ by z-test.

Table 1. *Morphological parameters for intermyofibrillar mitochondria in control and MV diaphragms*

Parameter	Diaphragm	Mean ± SE	Median, IQ	*P**
Aspect ratio	Control	2.64 ± 0.05	2.19, 1.52	
	MV	1.79 ± 0.03	1.48, 0.67	<0.001
Form factor	Control	1.88 ± 0.03	1.49, 0.91	
	MV	1.37 ± 0.02	1.15, 0.28	<0.001
Roundness, 0–1	Control	0.48 ± 0.01	0.46, 0.30	
	MV	0.65 ± 0.01	0.68, 0.27	<0.001
Feret's maximum diameter, μm	Control	1.02 ± 0.02	0.89, 0.62	
	MV	0.83 ± 0.02	0.74, 0.52	<0.001
Feret's minimum diameter, μm	Control	0.25 ± 0.004	0.21, 0.14	
	MV	0.26 ± 0.004	0.24, 0.17	0.01
Perimeter, μm	Control	2.55 ± 0.05	2.20, 1.50	
	MV	2.19 ± 0.04	1.97, 1.34	<0.001

MV, mechanically ventilated; SE, standard error; IQ, interquartile range. *Comparisons between control and MV by repeated-measures ANOVA.

values from the control group were used to subdivide the SS mitochondria populations from control (Fig. 3*C*) and MV (Fig. 3*D*) groups into four quadrants as we did for IMF mitochondria in Fig. 1. However, in marked contrast to the results of this analysis in IMF mitochondria, the proportion of SS mitochondria falling into the lower left-hand quadrant was identical (17%) in the control and MV groups.

Frequency distribution analyses in control and MV groups were next determined in the total SS mitochondrial population using the median value obtained in the control group as a reference threshold, as was performed for IMF mitochondria in Fig. 2. For aspect ratio and Feret's maximum diameter, there were slightly greater percentages of mitochondria with high values in the MV group compared with controls, whereas the opposite was true for roundness (Fig. 4). As shown in Table 2, the frequency distribution pattern was also associated with larger average values for Feret's maximum diameter (P = 0.03) and perimeter (P = 0.05) in MV vs. control SS mitochondria as determined by repeated-measures ANOVA. Therefore, morphological changes induced by MV in SS mitochondria were mild, and the overall pattern of changes was not consistent with the shift toward shorter and rounder mitochondria observed in the IMF population.

Mitochondrial interactions. IMF mitochondria are often observed in pairs flanking Z-lines in the longitudinal orientation, and less frequently as continuous organelles that cross the Z-line (Fig. 5, *A* and *B*). Mitochondria-mitochondria interactions can also be visualized as electron-dense IMJs between adjacent mitochondrial membranes (Fig. 5, *B* and *C*) (2, 44). The use of MV was associated with reductions in mitochondria crossing Z-lines in the IMF population (Fig. 5*D*). In addition,

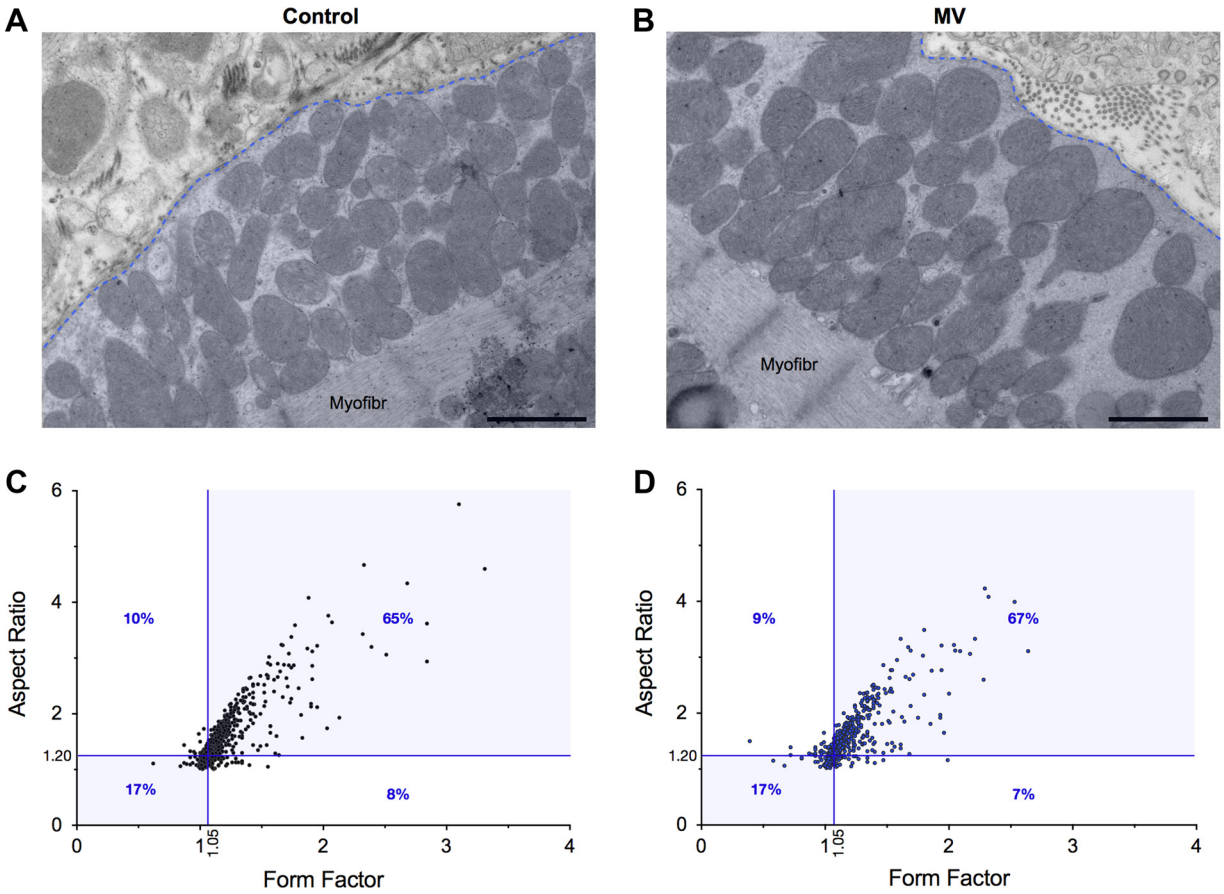

Fig. 3. MV does not fragment subsarcolemmal (SS) mitochondria. Representative electron micrographs from control (*A*) and MV (*B*) samples. The sarcolemma is marked by a dashed line, and cytoplasmic space of the myofiber is pseudocolored in blue. Scale bars = 1 μm. Myofibr indicates myofibrils. Graphical representation of mitochondrial form factor and aspect ratio in control (*C*) and MV (*D*) groups (n = 708 and 539 mitochondria for control and MV groups, respectively), with percentages indicating proportions of mitochondria within each quadrant defined by the 25th percentile of control mitochondria as described in Fig. 1.

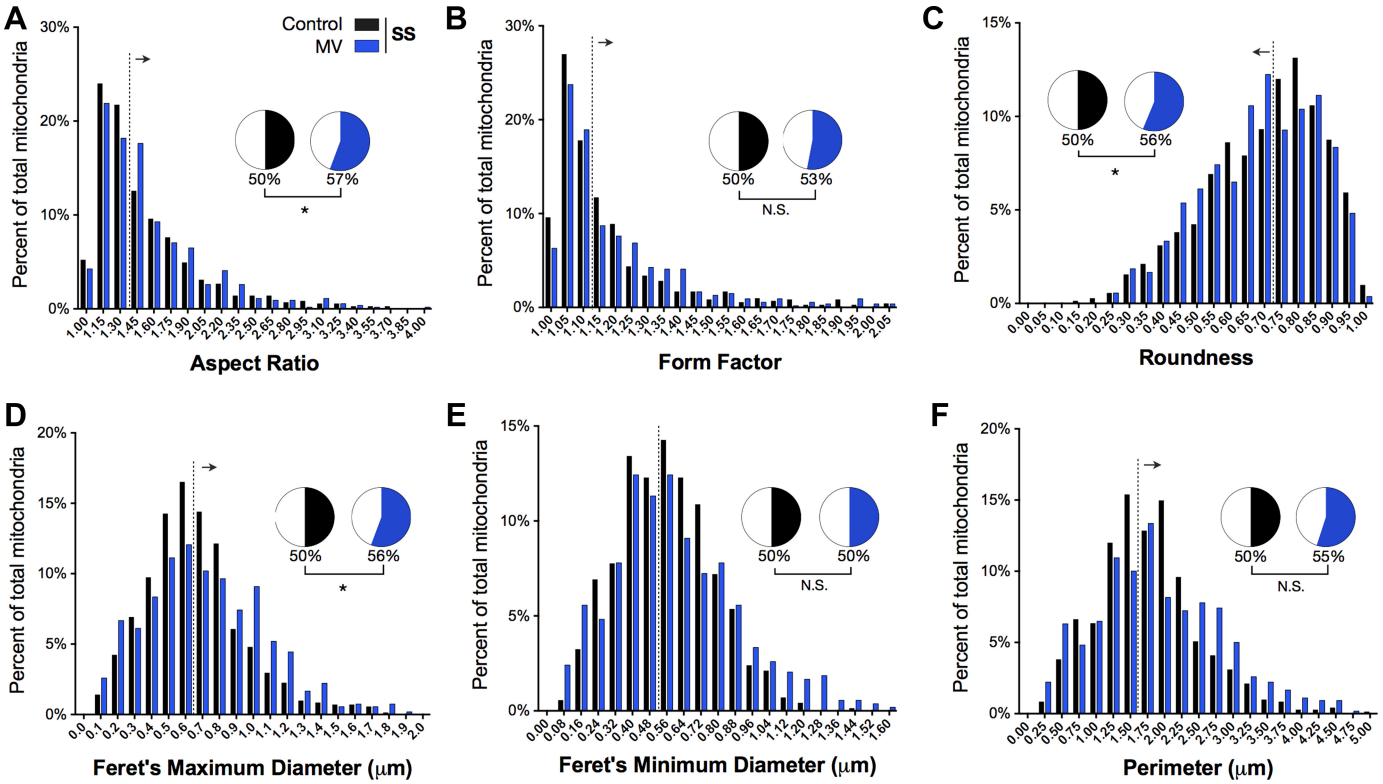

Fig. 4. MV has minimal effects on SS mitochondrial morphology. *A–F*: frequency distributions of the major SS mitochondrial shape and size descriptors in control and MV diaphragm. Vertical dashed lines represent median values in the control group from which proportions (shown in pie charts) were calculated as described in Fig. 2. *$P < 0.05$ by z-test. N.S., nonsignificant.

MV tended to decrease the proportion of IMJs between IMF mitochondria ($P = 0.06$), whereas IMJs between SS mitochondria (which were less abundant at baseline) did not show evidence of being affected by MV (Fig. 5*E*).

Proteins of mitochondrial dynamics. Western blot analysis of whole diaphragm tissue was performed to investigate the potential roles of mitochondrial profusion and profission proteins in mediating mitochondrial shape changes and mitochondrial membrane interactions induced by MV. There were no significant changes in the outer mitochondrial membrane profusion protein Mfn2 (Fig. 6*A*) or inner mitochondrial membrane profusion and organizing protein OPA1 (Fig. 6*B*) in the diaphragm following MV. However, the total amount of the mitochondrial fission protein Drp1 in diaphragm muscle was increased by MV (Fig. 6*C*). Phosphorylation of Drp1 at serines 616 (pDrp1-S616) and 637 (pDrp1-S637) are believed to activate and inhibit, respectively, the fission process initiated by Drp1 (51). The level of pDrp1-S616 in the diaphragm was increased by MV (Fig. 6*D*), whereas pDrp1-S637 remained unchanged (Fig. 6*E*). Furthermore, in MV group diaphragms, a significant increase in the proportion of very small mitochondria (less than or equal to the lower 5th percentile) was observed in the IMF population, whereas this was not the case for SS mitochondria (Fig. 6, *F* and *G*). Taken together, these findings support the presence of increased fission and associated fragmentation of mitochondria in the IMF population of the diaphragm during MV.

Table 2. *Morphological parameters for subsarcolemmal mitochondria in control and MV diaphragms*

Parameter	Diaphragm	Mean ± SE	Median, IQ	*P**
Aspect ratio	Control	1.55 ± 0.02	1.36, 0.50	
	MV	1.57 ± 0.02	1.44, 0.56	0.12
Form factor	Control	1.19 ± 0.01	1.11, 0.16	
	MV	1.20 ± 0.01	1.11, 0.22	0.68
Roundness, 0–1	Control	0.70 ± 0.01	0.73, 0.24	
	MV	0.69 ± 0.01	0.70, 0.25	0.13
Feret's maximum diameter, μm	Control	0.66 ± 0.01	0.62, 0.34	
	MV	0.72 ± 0.02	0.67, 0.50	0.03
Feret's minimum diameter, μm	Control	0.56 ± 0.008	0.55, 0.30	
	MV	0.60 ± 0.013	0.55, 0.39	0.11
Perimeter, μm	Control	1.78 ± 0.03	1.72, 0.90	
	MV	1.93 ± 0.04	1.79, 1.32	0.05

MV, mechanically ventilated; SE, standard error; IQ, interquartile range. *Comparisons between control and MV by repeated-measures ANOVA.

DISCUSSION

Mitochondria form a dynamic network that must be continuously adapted and tailored to the specific physiological requirements of different tissues. Such dynamic remodeling of the mitochondrial network requires the combined actions of fusion and fission, as well as interactions with other organelles and cytoskeletal components. These changes are mediated by the Mfn1/2 and OPA1 proteins, which promote fusion of the outer and inner mitochondrial membranes, respectively, whereas phosphorylation-dependent activation of the cytoplasmic dynamin-related protein Drp1 is largely responsible for mitochondrial fission (8, 51). In addition, Mfn2 plays a role in

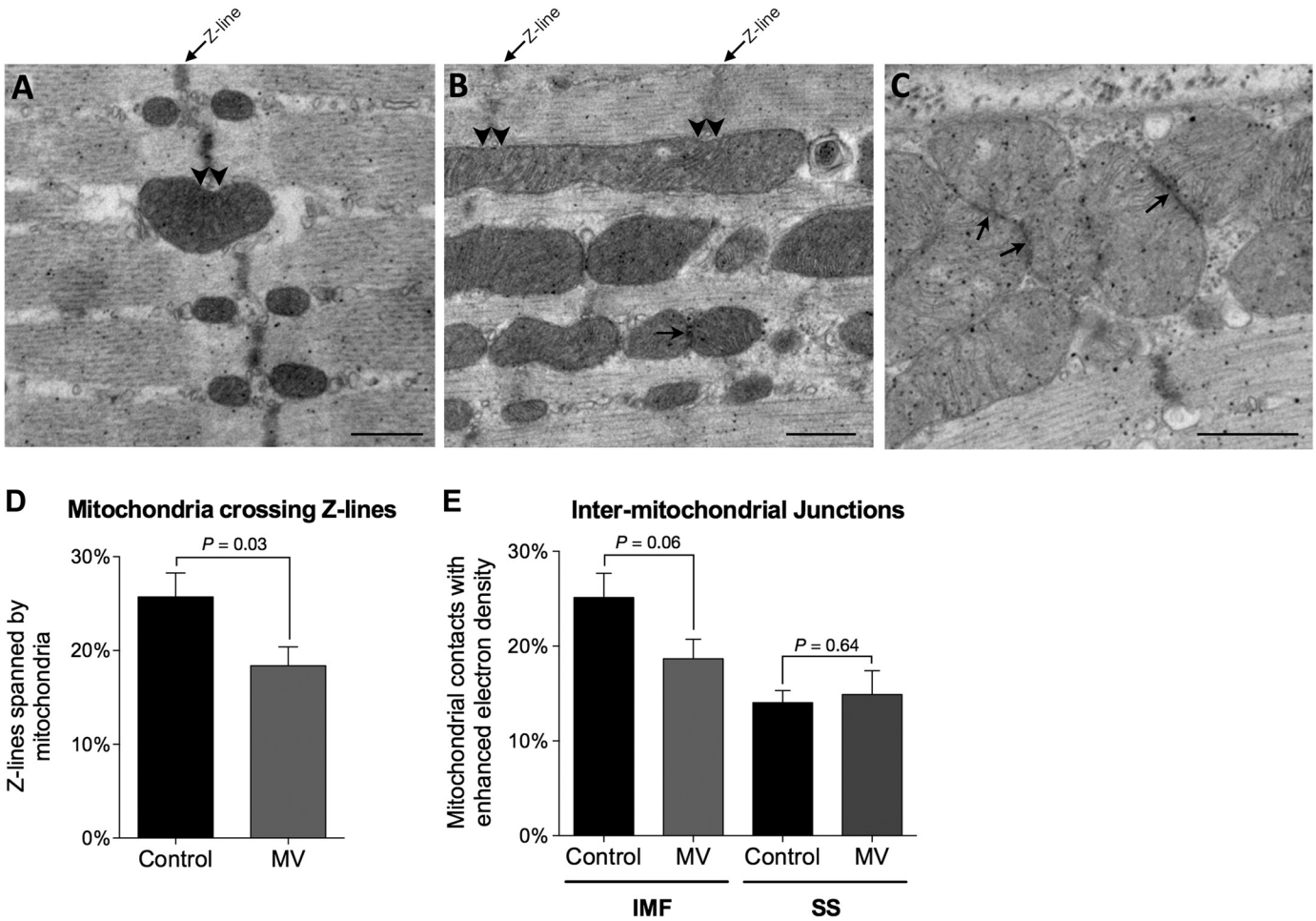

Fig. 5. MV reduces IMF mitochondrial membrane interactions. *A* and *B*: transmission electron microscopy images of diaphragm myofibers in longitudinal orientation showing several examples of mitochondria spanning Z-lines (double arrowheads). Electron-dense intermitochondrial junctions (IMJs) between adjacent IMF (*B*) and SS (*C*) mitochondria are also shown (arrows). *D*: proportion of IMF mitochondria interacting across Z-lines in control and MV diaphragms. *E*: proportion of mitochondrial IMJs in IMF and SS mitochondria in control and MV diaphragms. Scale bars = 500 nm.

the regulation of mitochondrial tethering to other organelles, such as the endoplasmic reticulum (13).

In the present study, we employed quantitative electron microscopy to assess mitochondrial morphological remodeling in the diaphragm following application of a well-established model of VIDD, consisting of 6 h of controlled MV in mice (37). We separately analyzed the IMF and SS mitochondrial populations, which are known to exhibit different functional properties and responses to various physiological perturbations (1, 12, 29, 38, 42). Our major findings are that in response to MV, the IMF (but not the SS) mitochondrial population in the diaphragm undergoes major shape changes (becoming significantly shorter, rounder, and less morphologically complex) and also contains a higher proportion of very small mitochondria, consistent with mitochondrial fragmentation. Furthermore, simultaneously higher levels of activated Drp1 (pDrp1-S616) protein in the diaphragm without any changes in either Mfn2 or OPA1 provide additional biochemical evidence for a net shift in mitochondrial dynamics toward induction of the mitochondrial fission-fragmentation pathway during MV.

There is substantial evidence that mitochondrial health and normal skeletal muscle function depend on continually maintaining a finely tuned balance between fusion and fission events (8, 51). Disruption of this equilibrium can lead to decreased mitochondrial respiratory capacity (9, 26, 56), greater susceptibility to apoptosis (31, 39), and failure to appropriately eliminate or recycle damaged mitochondria (50). In rat skeletal muscle cells, silencing of Mfn2 and OPA1 attenuated insulin-stimulated Akt phosphorylation and cellular respiratory rate (14). Along the same lines, decreased Mfn1/2 and increased Drp1 were associated with impaired mitochondrial respiration and reduced ATP levels in the skeletal muscles of mice with high-fat-diet-induced obesity (34). The latter findings are consistent with reports of decreased Mfn2 and smaller mitochondria in skeletal muscles of obese and diabetic patients (3, 21). Excessive mitochondrial fission has also been linked to mitochondrial dysfunction and insulin resistance in mouse skeletal muscle (26), and to greater mitochondrial ROS release and less ability to resist mitochondrial permeability transition pore opening in other cell types (45, 56). Moreover, there is evidence that exaggerated mitochondrial fission-fragmentation is a stimulus for activation of muscle atrophy pathways (48).

Mitochondrial fusion and fission occur within seconds to minutes in various types of cultured cells in vitro, and a rapid time course of mitochondrial dynamics has also recently been

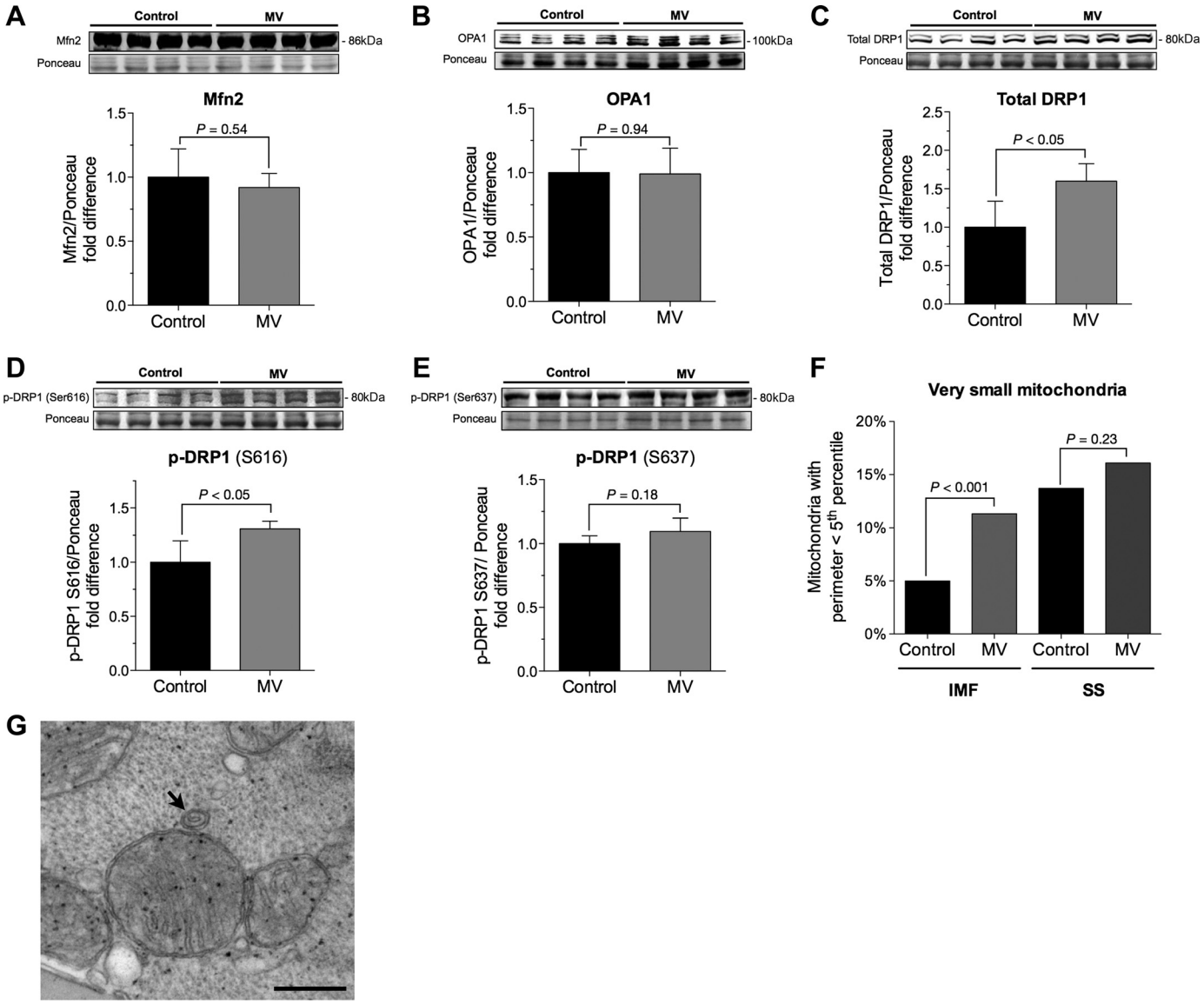

Fig. 6. Effect of MV on mitochondrial profission and profusion proteins. Abundance of profusion proteins mitofusin 2 (Mfn2, *A*) and optic atrophy 1 (OPA1, *B*). *C*: abundance of profission dynamin-related protein 1 (DRP1) and its phosphorylated forms p-DRP1 Ser616 (*D*) and p-DRP1 Ser637 (*E*); groups were compared by *t*-test. *F*: proportion of very small mitochondria in IMF and SS compartments (based on 5th percentile value for control IMF mitochondria); groups were compared by z-test. *G*: representative image showing very small mitochondrion (arrow) in the diaphragm of a mouse that underwent MV. Scale bar = 200 nm.

demonstrated in adult skeletal muscle fibers (16, 34). However, very little work has been published regarding changes in mitochondrial dynamics induced by skeletal muscle disuse in vivo. In rodents, denervation (24, 54) and hind limb unloading (7, 53) have been reported to downregulate either OPA1, or Mfn2, or both. The present investigation is to our knowledge the first in any skeletal muscle disuse model to demonstrate through a quantitative morphometric analysis that skeletal muscle inactivity produces signs of exaggerated mitochondrial fission-fragmentation in vivo.

Beyond fusion and fission events, dynamic remodeling of the mitochondrial network is also influenced by mitochondrial interactions with other cellular organelles. In the present study, we observed evidence of reduced mitochondrial interactions across Z-lines following diaphragm inactivity induced by MV, and electron-dense IMJs (2, 44) between adjacent mitochondria also tended to be less frequent in MV group diaphragms. Interestingly, voluntary running was recently shown to significantly increase the prevalence of IMJs between neighboring mitochondria in mouse soleus muscle (42). In addition to the potential effect on mitochondrial shape, a reduction in such interorganellar interactions would be expected to disrupt functional cross-talk between mitochondria and other cellular constituents. For example, there is evidence that contacts between mitochondria and the sarcoplasmic reticulum are critically involved in normal Ca^{2+} handling (15), and it was recently reported that Mfn1 depletion interferes with ryanodine receptor-mediated excitation-contraction coupling (16). It is conceivable that mitochondria-mitochondria interactions and the transmitochondrial coordination of mitochondrial ultrastructure (44) can similarly play a role in electrochemical coupling between neighboring mitochondria (2).

On the basis of their different localization and functional properties, it has been hypothesized that IMF mitochondria play the dominant role in supplying ATP for muscle contraction, whereas SS mitochondria are likely to be more involved in sarcolemmal membrane-associated functions (30). Previous studies have established that IMF mitochondria, which constitute ~80% of mitochondria in skeletal muscle, possess a higher oxidative capacity than SS mitochondria (11, 41). Few studies have examined whether skeletal muscle disuse differentially affects IMF and SS mitochondria, and these prior investigations have provided conflicting results with regard to which mitochondrial population is more vulnerable to disuse effects (18, 29, 38). In our study, major morphological alterations occurred in IMF mitochondria, whereas the SS population exhibited relatively few and minor changes in response to MV. It is interesting to note that the general direction of changes observed in IMF mitochondria was toward the more spheroid and morphologically simple characteristics of the SS mitochondrial population. This finding suggests that diaphragm inactivity blunts the specialized morphological features associated with IMF mitochondria, thus making the two mitochondrial subpopulations more homogeneous. The reason for a greater susceptibility of the IMF population to MV is unclear, but could be related to its naturally more complex and wide range of morphology (46), its larger role in ATP-driven muscle contraction, and the fact that IMF mitochondria are more sensitive to ROS-induced proapoptotic protein release (1).

An important question raised by our study is how the mitochondrial morphological abnormalities we have documented in the mechanically ventilated diaphragm might be causally related to mitochondrial and contractile dysfunction in the muscle. A cardinal feature of VIDD pathogenesis is increased oxidative stress derived in large part from mitochondria (27, 36, 43, 47). Cell culture studies have demonstrated that mitochondrial fission-fragmentation can trigger increased mitochondrial ROS emission (56), and greater oxidative stress can also provoke mitochondrial fragmentation (17), suggesting the potential for a deleterious feed-forward loop. In addition, either inhibition of mitochondrial fission or promotion of mitochondrial fusion can blunt the increased ROS production triggered by metabolic overload with high glucose and lipid exposure (26, 56). This is of interest because hyperglycemia has been linked to diaphragmatic oxidative stress and respiratory muscle dysfunction in animals (6) and humans during MV (20). We have also previously reported evidence of metabolic substrate overload in diaphragm muscle fibers of mechanically ventilated patients and found that hyperlipidemia exacerbates oxidative stress in parallel with contractile dysfunction (43). Nevertheless, it is important to recognize that although a mechanistic link between mitochondrial fragmentation and VIDD is biologically plausible and consistent with the findings of our study, this hypothesis remains to be formally tested. This will likely require the use of genetically modified mice either deficient or overexpressing the major proteins of mitochondrial dynamics to perform a simultaneous analysis of mitochondrial dynamics, mitochondrial ROS production, and diaphragm contractility outcomes. In addition, it will be of interest to ascertain how mitochondrial dynamics are affected after more prolonged periods of MV, when diaphragmatic muscle atrophy becomes a prominent feature.

In summary, this study has demonstrated for the first time that an early abnormality of mitochondrial structure during MV consists of the loss of regionally specialized morphological characteristics within the IMF mitochondrial population, which lies in closest contact with the contractile apparatus and constitutes the bulk of skeletal muscle mitochondria. The physical alterations found in IMF mitochondria during MV suggest a major dysequilibrium of mitochondrial dynamics in favor of exaggerated fission-fragmentation. Most of the cellular events demonstrated to be causally involved in the development of diaphragmatic weakness during MV can be mechanistically linked to mitochondrial dysfunction. Given this fact together with accumulating evidence of an intimate relationship between mitochondrial morphology transitions and canonical aspects of the organelle's function (45), it is possible that dysregulated mitochondrial dynamics play a significant role in the pathogenesis of VIDD. This remains to be determined by future studies, and it will also be of interest to ascertain whether mitochondrial dynamics are affected by other known modifiers of VIDD such as metabolic substrate supply (43), ROS scavengers (47), and the use of partial support modes of MV (19).

GRANTS

Support for this study was provided by a Canadian Institutes of Health Research (CIHR) Postdoctoral Fellowship to M. Picard from the Institute of Neurosciences, Mental Health and Addiction as part of the Canadian Epigenetics, Environment and Health Research Consortium; B. Jung was supported by Société Française d'Anesthésie Réanimation and Association Pour l'Assistance et la Réhabilitation à Domicile. Support for this study was also provided by grants from CIHR and the McGill University Health Centre Research Institute to B.J. Petrof and Y. Burelle.

DISCLOSURES

No conflicts of interest, financial or otherwise, are declared by the authors.

AUTHOR CONTRIBUTIONS

M.P., S.M., S.H., Y.B., and B.J.P. conception and design of research; M.P., I.A., B.J., K.W., T.L., F.L., and B.J.G. performed experiments; M.P., I.A., C.G., and A.B. analyzed data; M.P., I.A., and B.J.P. interpreted results of experiments; M.P. and I.A. prepared figures; M.P. drafted manuscript; M.P., B.J.G., Y.B., and B.J.P. edited and revised manuscript; M.P., I.A., B.J., C.G., S.M., S.H., K.W., T.L., F.L., A.B., B.J.G., Y.B., and B.J.P. approved final version of manuscript.

REFERENCES

1. **Adhihetty PJ, Ljubicic V, Menzies KJ, Hood DA.** Differential susceptibility of subsarcolemmal and intermyofibrillar mitochondria to apoptotic stimuli. *Am J Physiol Cell Physiol* 289: C994–C1001, 2005.
2. **Amchenkova AA, Bakeeva LE, Chentsov YS, Skulachev VP, Zorov DB.** Coupling membranes as energy-transmitting cables. I. Filamentous mitochondria in fibroblasts and mitochondrial clusters in cardiomyocytes. *J Cell Biol* 107: 481–495, 1988.
3. **Bach D, Naon D, Pich S, Soriano FX, Vega N, Rieusset J, Laville M, Guillet C, Boirie Y, Wallberg-Henriksson H, Manco M, Calvani M, Castagneto M, Palacin M, Mingrone G, Zierath JR, Vidal H, Zorzano A.** Expression of Mfn2, the Charcot-Marie-Tooth neuropathy type 2A gene, in human skeletal muscle: effects of type 2 diabetes, obesity, weight loss, and the regulatory role of tumor necrosis factor alpha and interleukin-6. *Diabetes* 54: 2685–2693, 2005.
4. **Bakeeva LE, Chentsov Yu S, Skulachev VP.** Mitochondrial framework (reticulum mitochondriale) in rat diaphragm muscle. *Biochim Biophys Acta* 501: 349–369, 1978.
5. **Benard G, Bellance N, Jose C, Melser S, Nouette-Gaulain K, Rossignol R.** Multi-site control and regulation of mitochondrial energy production. *Biochim Biophys Acta* 1797: 698–709, 2010.

6. **Callahan LA, Supinski GS.** Hyperglycemia-induced diaphragm weakness is mediated by oxidative stress. *Crit Care* 18: R88, 2014.
7. **Cannavino J, Brocca L, Sandri M, Grassi B, Bottinelli R, Pellegrino MA.** The role of alterations in mitochondrial dynamics and PGC-1alpha over-expression in fast muscle atrophy following hindlimb unloading. *J Physiol*. First published January 7, 2015; doi: 10.1113/jphysiol.2014.286740.
8. **Chan DC.** Fusion and fission: interlinked processes critical for mitochondrial health. *Annu Rev Genet* 46: 265–287, 2012.
9. **Chen H, Chomyn A, Chan DC.** Disruption of fusion results in mitochondrial heterogeneity and dysfunction. *J Biol Chem* 280: 26185–26192, 2005.
10. **Chen H, Vermulst M, Wang YE, Chomyn A, Prolla TA, McCaffery JM, Chan DC.** Mitochondrial fusion is required for mtDNA stability in skeletal muscle and tolerance of mtDNA mutations. *Cell* 141: 280–289, 2010.
11. **Cogswell AM, Stevens RJ, Hood DA.** Properties of skeletal muscle mitochondria isolated from subsarcolemmal and intermyofibrillar regions. *Am J Physiol Cell Physiol* 264: C383–C389, 1993.
12. **Crescenzo R, Bianco F, Coppola P, Mazzoli A, Liverini G, Iossa S.** Subsarcolemmal and intermyofibrillar mitochondrial responses to short-term high-fat feeding in rat skeletal muscle. *Nutrition* 30: 75–81, 2014.
13. **de Brito OM, Scorrano L.** Mitofusin 2 tethers endoplasmic reticulum to mitochondria. *Nature* 456: 605–610, 2008.
14. **del Campo A, Parra V, Vásquez-Trincado C, Gutiérrez T, Morales PE, López-Crisosto C, Bravo-Sagua R, Navarro-Marquez MF, Verdejo HE, Contreras-Ferrat A, Troncoso R, Chiong M, Lavandero S.** Mitochondrial fragmentation impairs insulin-dependent glucose uptake by modulating Akt activity through mitochondrial Ca^{2+} uptake. *Am J Physiol Endocrinol Metab* 306: E1–E13, 2014.
15. **Eisner V, Csordás G, Hajnóczky G.** Interactions between sarco-endoplasmic reticulum and mitochondria in cardiac and skeletal muscle - pivotal roles in Ca(2)(+) and reactive oxygen species signaling. *J Cell Sci* 126: 2965–2978, 2013.
16. **Eisner V, Lenaers G, Hajnóczky G.** Mitochondrial fusion is frequent in skeletal muscle and supports excitation-contraction coupling. *J Cell Biol* 205: 179–195, 2014.
17. **Fan X, Hussien R, Brooks GA.** H2O2-induced mitochondrial fragmentation in C2C12 myocytes. *Free Radic Biol Med* 49: 1646–1654, 2010.
18. **Ferretti G, Antonutto G, Denis C, Hoppeler H, Minetti AE, Narici MV, Desplanches D.** The interplay of central and peripheral factors in limiting maximal O2 consumption in man after prolonged bed rest. *J Physiol* 501, *Pt* 3: 677–686, 1997.
19. **Futier E, Constantin JM, Combaret L, Mosoni L, Roszyk L, Sapin V, Attaix D, Jung B, Jaber S, Bazin JE.** Pressure support ventilation attenuates ventilator-induced protein modifications in the diaphragm. *Crit Care* 12: R116, 2008.
20. **Hermans G, Wilmer A, Meersseman W, Milants I, Wouters PJ, Bobbaers H, Bruyninckx F, Van den Berghe G.** Impact of intensive insulin therapy on neuromuscular complications and ventilator dependency in the medical intensive care unit. *Am J Respir Crit Care Med* 175: 480–489, 2007.
21. **Hernández-Alvarez MI, Thabit H, Burns N, Shah S, Brema I, Hatunic M, Finucane F, Liesa M, Chiellini C, Naon D, Zorzano A, Nolan JJ.** Subjects with early-onset type 2 diabetes show defective activation of the skeletal muscle PGC-1{alpha}/Mitofusin-2 regulatory pathway in response to physical activity. *Diabetes Care* 33: 645–651, 2010.
22. **Hooijman PE, Beishuizen A, de Waard MC, de Man FS, Vermeijden JW, Steenvoorde P, Bouwman RA, Lommen W, van Hees HW, Heunks LM, Dickhoff C, van der Peet DL, Girbes AR, Jasper JR, Malik FI, Stienen GJ, Hartemink KJ, Paul MA, Ottenheijm CA.** Diaphragm fiber strength is reduced in critically ill patients and restored by a troponin activator. *Am J Respir Crit Care Med* 189: 863–865, 2014.
23. **Hussain SN, Mofarrahi M, Sigala I, Kim HC, Vassilakopoulos T, Maltais F, Bellenis I, Chaturvedi R, Gottfried SB, Metrakos P, Danialou G, Matecki S, Jaber S, Petrof BJ, Goldberg P.** Mechanical ventilation-induced diaphragm disuse in humans triggers autophagy. *Am J Respir Crit Care Med* 182: 1377–1386, 2010.
24. **Iqbal S, Ostojic O, Singh K, Joseph AM, Hood DA.** Expression of mitochondrial fission and fusion regulatory proteins in skeletal muscle during chronic use and disuse. *Muscle Nerve* 48: 963–970, 2013.
25. **Jaber S, Jung B, Matecki S, Petrof BJ.** Clinical review: ventilator-induced diaphragmatic dysfunction–human studies confirm animal model findings! *Crit Care* 15: 206, 2011.
26. **Jheng HF, Tsai PJ, Guo SM, Kuo LH, Chang CS, Su IJ, Chang CR, Tsai YS.** Mitochondrial fission contributes to mitochondrial dysfunction and insulin resistance in skeletal muscle. *Mol Cell Biol* 32: 309, 2012.
27. **Kavazis AN, Talbert EE, Smuder AJ, Hudson MB, Nelson WB, Powers SK.** Mechanical ventilation induces diaphragmatic mitochondrial dysfunction and increased oxidant production. *Free Radic Biol Med* 46: 842–850, 2009.
28. **Koopman WJ, Visch HJ, Smeitink JA, Willems PH.** Simultaneous quantitative measurement and automated analysis of mitochondrial morphology, mass, potential, and motility in living human skin fibroblasts. *Cytometry A* 69: 1–12, 2006.
29. **Krieger DA, Tate CA, McMillin-Wood J, Booth FW.** Populations of rat skeletal muscle mitochondria after exercise and immobilization. *J Appl Physiol* 48: 23–28, 1980.
30. **Lawrie AM, Rizzuto R, Pozzan T, Simpson AW.** A role for calcium influx in the regulation of mitochondrial calcium in endothelial cells. *J Biol Chem* 271: 10753–10759, 1996.
31. **Lee YJ, Jeong SY, Karbowski M, Smith CL, Youle RJ.** Roles of the mammalian mitochondrial fission and fusion mediators Fis1, Drp1, and Opa1 in apoptosis. *Mol Biol Cell* 15: 5001–5011, 2004.
32. **Levine S, Biswas C, Dierov J, Barsotti R, Shrager JB, Nguyen T, Sonnad S, Kucharchzuk JC, Kaiser LR, Singhal S, Budak MT.** Increased proteolysis, myosin depletion and atrophic AKT-FOXO signaling in human diaphragm disuse. *Am J Respir Crit Care Med* 183: 483–490, 2010.
33. **Levine S, Nguyen T, Taylor N, Friscia ME, Budak MT, Rothenberg P, Zhu J, Sachdeva R, Sonnad S, Kaiser LR, Rubinstein NA, Powers SK, Shrager JB.** Rapid disuse atrophy of diaphragm fibers in mechanically ventilated humans. *N Engl J Med* 358: 1327–1335, 2008.
34. **Liu R, Jin P, LiqunYu Wang Y, Han L, Shi T, Li X.** Impaired mitochondrial dynamics and bioenergetics in diabetic skeletal muscle. *PLoS One* 9: e92810, 2014.
35. **McClung JM, Kavazis AN, DeRuisseau KC, Falk DJ, Deering MA, Lee Y, Sugiura T, Powers SK.** Caspase-3 regulation of diaphragm myonuclear domain during mechanical ventilation-induced atrophy. *Am J Respir Crit Care Med* 175: 150–159, 2007.
36. **McClung JM, Whidden MA, Kavazis AN, Falk DJ, Deruisseau KC, Powers SK.** Redox regulation of diaphragm proteolysis during mechanical ventilation. *Am J Physiol Regul Integr Comp Physiol* 294: R1608–R1617, 2008.
37. **Mrozek S, Jung B, Petrof BJ, Pauly M, Roberge S, Lacampagne A, Cassan C, Thireau J, Molinari N, Futier E, Scheuermann V, Constantin JM, Matecki S, Jaber S.** Rapid onset of specific diaphragm weakness in a healthy murine model of ventilator-induced diaphragmatic dysfunction. *Anesthesiology* 117: 560–567, 2012.
38. **Nielsen J, Suetta C, Hvid LG, Schroder HD, Aagaard P, Ortenblad N.** Subcellular localization-dependent decrements in skeletal muscle glycogen and mitochondria content following short-term disuse in young and old men. *Am J Physiol Endocrinol Metab* 299: E1053–E1060, 2010.
39. **Ong SB, Subrayan S, Lim SY, Yellon DM, Davidson SM, Hausenloy DJ.** Inhibiting mitochondrial fission protects the heart against ischemia/reperfusion injury. *Circulation* 121: 2012–2022, 2010.
40. **Ono T, Isobe K, Nakada K, Hayashi JI.** Human cells are protected from mitochondrial dysfunction by complementation of DNA products in fused mitochondria. *Nat Genet* 28: 272–275, 2001.
41. **Palmer JW, Tandler B, Hoppel CL.** Biochemical differences between subsarcolemmal and interfibrillar mitochondria from rat cardiac muscle: effects of procedural manipulations. *Arch Biochem Biophys* 236: 691–702, 1985.
42. **Picard M, Gentil BJ, McManus MJ, White K, St Louis K, Gartside SE, Wallace DC, Turnbull DM.** Acute exercise remodels mitochondrial membrane interactions in mouse skeletal muscle. *J Appl Physiol* 115: 1562–1571, 2013.
43. **Picard M, Jung B, Liang F, Azuelos I, Hussain S, Goldberg P, Godin R, Danialou G, Chaturvedi R, Rygiel K, Matecki S, Jaber S, Des Rosiers C, Karpati G, Ferri L, Burelle Y, Turnbull DM, Taivassalo T, Petrof BJ.** Mitochondrial dysfunction and lipid accumulation in the human diaphragm during mechanical ventilation. *Am J Respir Crit Care Med* 186: 1140–1149, 2012.
44. **Picard M, McManus MJ, Csordas G, Várnai P, Dorn Li GW, Williams D, Hajnóczky G, Wallace DC.** Trans-mitochondrial coordination of cristae at regulated membrane junctions. *Nat Commun* 6: 6259, 2015.

45. **Picard M, Shirihai OS, Gentil BJ, Burelle Y.** Mitochondrial morphology transitions and functions: implications for retrograde signaling? *Am J Physiol Regul Integr Comp Physiol* 304: R393–R406, 2013.
46. **Picard M, White K, Turnbull DM.** Mitochondrial morphology, topology, and membrane interactions in skeletal muscle: a quantitative three-dimensional electron microscopy study. *J Appl Physiol* 114: 161–171, 2013.
47. **Powers SK, Hudson MB, Nelson WB, Talbert EE, Min K, Szeto HH, Kavazis AN, Smuder AJ.** Mitochondria-targeted antioxidants protect against mechanical ventilation-induced diaphragm weakness. *Crit Care Med* 39: 1749–1759, 2011.
48. **Romanello V, Guadagnin E, Gomes L, Roder I, Sandri C, Petersen Y, Milan G, Masiero E, Del Piccolo P, Foretz M, Scorrano L, Rudolf R, Sandri M.** Mitochondrial fission and remodelling contributes to muscle atrophy. *EMBO J* 29: 1774–1785, 2010.
49. **Tang H, Lee M, Budak MT, Pietras N, Hittinger S, Vu M, Khuong A, Hoang CD, Hussain SN, Levine S, Shrager JB.** Intrinsic apoptosis in mechanically ventilated human diaphragm: linkage to a novel Fos/FoxO1/Stat3-Bim axis. *FASEB J* 25: 2921–2936, 2011.
50. **Twig G, Elorza A, Molina AJ, Mohamed H, Wikstrom JD, Walzer G, Stiles L, Haigh SE, Katz S, Las G, Alroy J, Wu M, Py BF, Yuan J, Deeney JT, Corkey BE, Shirihai OS.** Fission and selective fusion govern mitochondrial segregation and elimination by autophagy. *EMBO J* 27: 433–446, 2008.
51. **van der Bliek AM, Shen Q, Kawajiri S.** Mechanisms of mitochondrial fission and fusion. *Cold Spring Harbor Perspect Biol* 5: 2013.
52. **Vassilakopoulos T, Petrof BJ.** Ventilator-induced diaphragmatic dysfunction. *Am J Respir Crit Care Med* 169: 336–341, 2004.
53. **Wagatsuma A, Kotake N, Kawachi T, Shiozuka M, Yamada S, Matsuda R.** Mitochondrial adaptations in skeletal muscle to hindlimb unloading. *Mol Cell Biochem* 350: 1–11, 2011.
54. **Wagatsuma A, Kotake N, Mabuchi K, Yamada S.** Expression of nuclear-encoded genes involved in mitochondrial biogenesis and dynamics in experimentally denervated muscle. *J Physiol Biochem* 67: 359–370, 2011.
55. **Wasilewski M, Scorrano L.** The changing shape of mitochondrial apoptosis. *Trends Endocrinol Metab* 20: 287–294, 2009.
56. **Yu T, Sheu SS, Robotham JL, Yoon Y.** Mitochondrial fission mediates high glucose-induced cell death through elevated production of reactive oxygen species. *Cardiovasc Res* 79: 341–351, 2008.